metals

MDPI

Article

Effects of Sheared Edge and Overlap Length on Reduction in Tensile Fatigue Limit before and after Hydrogen Embrittlement of Resistance Spot-Welded Ultra-High-Strength Steel Sheets

Ryo Yagita * and Yohei Abe

Department of Mechanical Engineering, Toyohashi University of Technology, Toyohashi 441-8580, Japan; abe@me.tut.ac.jp
* Correspondence: yagita@plast.me.tut.ac.jp

Abstract: The effects of a sheared edge and overlap length on the reduction in the tensile fatigue limit before and after hydrogen embrittlement of resistance spot-welded ultra-high-strength steel sheets were investigated. Ultra-high-strength steel sheets with sheared and laser-cut edges were subjected to resistance spot welding followed by hydrogen embrittlement via cathodic hydrogen charging and subjected to static tensile shear and fatigue tests. The distance between the resistance spot weld and the sheared and laser-cut edges was changed by changing the overlap length, and the influence of the weld position was investigated. In the tensile shear test, the maximum load decreased with decreasing overlap length and the maximum load decreased with hydrogen embrittlement, but the effect of hydrogen embrittlement was smaller than that in the fatigue test. In the fatigue test, the fatigue mode changed from the width direction to the sheared edge direction with the increase in the repeated load. Even if the overlap length was reduced, the fracture changed to the sheared edge direction. In the specimens with sheared edges, the effect of fatigue limit reduction due to hydrogen embrittlement was greater than in the specimens with laser surfaces. In particular, the effect was greatest when the fatigue mode was changed via hydrogen embrittlement.

Keywords: shearing; ultra-high-strength steel; resistance spot welding; hydrogen embrittlement; JSC1180

check for updates

Citation: Yagita, R.; Abe, Y. Effects of Sheared Edge and Overlap Length on Reduction in Tensile Fatigue Limit before and after Hydrogen Embrittlement of Resistance Spot-Welded Ultra-High-Strength Steel Sheets. *Metals* **2023**, *13*, 2002. https://doi.org/10.3390/met13122002

Academic Editors: Jonas Hensel and Kevin Höfer

Received: 13 September 2023
Revised: 7 November 2023
Accepted: 16 November 2023
Published: 12 December 2023

1. Introduction

To improve the fuel consumption of automobiles, a reduction in the weight of automobiles is required in the automobile industry. To reduce the weight, the application of high-strength and ultra-high-strength steel sheets with small thicknesses to automotive body parts is increasing. Ultra-high-strength steel sheets with a tensile strength above 1000 MPa are widely applied in the automotive body parts and aerospace industries due to their high strength. However, large forming load [1], very large springback [2], small formability [3], tool failure [4], and hydrogen-induced delayed fracture [5] are problematic in the cold stamping of ultra-high-strength steel sheets.

Factors that contribute to delayed hydrogen embrittlement fracture include microstructure [6], surface conditions [7], phase structure [8], and tensile residual stress. Although coatings are able to reduce hydrogen sensitivity [9], coatings also reduce weldability. In addition to laser and arc spot welding, resistance spot welding is widely used for assembling automobile bodies [10,11].

Liquid metal embrittlement (LME), which is a major problem in the resistance spot welding of ultra-high-strength steel sheets, has been investigated in terms of the effects of microstructure, coatings, and other factors. The radius of curvature has an effect on the LME because the electrode is cooled from its contact surface with the curved surface [12,13]. As for metallurgical structures, it has been shown that LME occurs more easily in high-strength steels than in low-carbon steels [14], and that a high silicone content in dual-phase steels increases LME sensitivity [15].

In resistance spot welding, welding current has a large influence on welding conditions. In annealed plated steel, an increase in welding current is necessary to increase the heat value [16]. In welding TWIP steel, an increase in welding current worsens the LME [17] but reduces the tensile residual stress in the weld [18]. Simulations of welding DX56D steel sheets show that the tensile residual stresses in the resistance spot welds cause warpage deformation in the steel sheets, which affects the assembly of the parts [19].

Studies have been conducted to improve the fatigue limit of resistance spot welds. It has been shown that fatigue strength increases with increasing nugget diameter and compressive residual stress [20], that fatigue strength increases with the relaxation of tensile residual stress in 980 MPa-class steel [21], and that cracks develop from the boundary between the nugget and heat-affected zone [22]. In a resistance spot-welded AISI 304 steel sheet, the tensile shear fatigue strength at 10^7 times decreased by about 20% with an R value from 0.05 to 0.67 [23]. In addition, the fatigue strength of AISI 304 and SAF 2304 under a NaCl environment decreased by about 30~40% compared with that under an atmospheric environment [24]. The fatigue strength of resistance spot-welded combinations of galvanized steel sheets and AISI 304 was lower than that of welding two sheets of each steel sheet together [25]. Different crack extension directions were observed for resistance spot-welded DP600GI and HSLA340Y GI at different fatigue loads [26]. Post-weld cold working (PWCW) of DP980 resistance spot welds increased fatigue strength due to compressive stresses [27]. The experimentally measured crack extension angles were compared with the numerical results for a 590 MPa steel sheet, and the results were closer to the experimental values than to the theoretical values [28].

Hydrogen embrittlement and various types of joining are also being studied. In K-TIG-welded AISI 304 SS, the tensile fracture mode changed when it was charged with hydrogen at current densities above 50 mA/cm^2 [29]. The effect of hydrogen in the stir zone was smaller in friction–diffusion-welded low-carbon steel than in the base metal [30].

The manufacturing process of an automobile body is shown in Figure 1, and cracking due to hydrogen embrittlement-delayed fracture at the sheared edge and resistance spot welds is shown in Figure 2. Tensile residual stresses occur in blanking and resistance spot welding. Therefore, hydrogen in the environment can cause hydrogen embrittlement-delayed fracture. On the other hand, the distance to a cut edge in an automotive body is closer than in material testing, and the effect of a cut edge is more likely to occur. Fatigue strength in long-term use is also important. However, there are no papers that examine the effects of cut surfaces and overlap on the fatigue strength of hydrogen-embrittled ultra-high-strength steel sheets, which should be evaluated to expand the use of ultra-high-strength steel sheets.

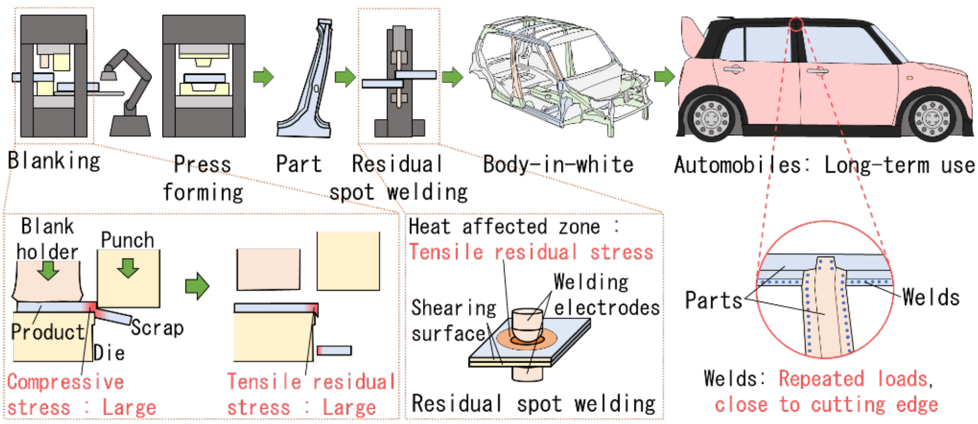

Figure 1. Manufacturing process of an automobile body.

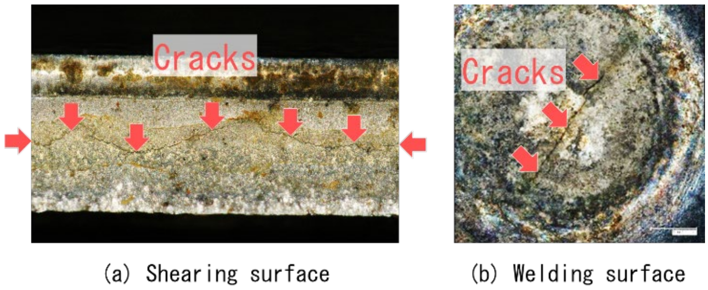

Figure 2. Cracks due to hydrogen embrittlementdelayed fracture at (**a**) sheared edge and (**b**) resistance spot welds.

In this paper, tensile fatigue specimens with different cutting edges and overlaps were hydrogen-charged to observe the effects of sheared edge and overlap length on fatigue strength before and after hydrogen embrittlement.

2. Materials and Methods

The test method in this study is shown in Figure 3. Sheets were cut using laser cutting and shearing, and then resistance spot-welded with a different overlap length. The specimens were hydrogen-charged with the cathodic hydrogen charge test, and changes in tensile shear strength and fatigue strength were measured with the tensile shear test and shear fatigue test, and the effects of the cut edge and overlap length were examined.

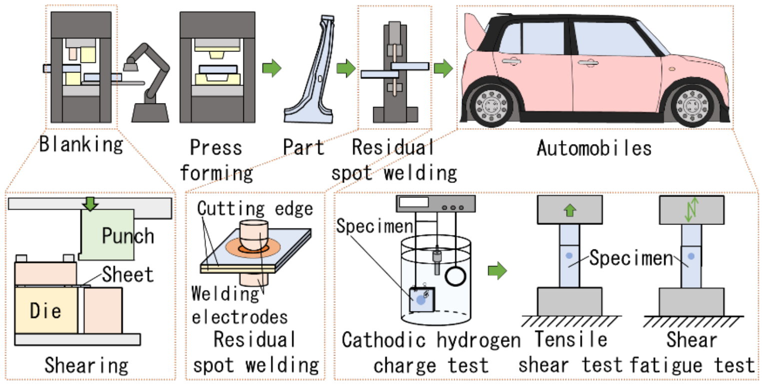

Figure 3. Test method in this study.

The mechanical properties of the sheet used are shown in Table 1. A sheet with a nominal tensile strength of 1180 MPa was used. The steel sheet was a dual-phase and non-coating sheet. The nominal thickness was 1.2 mm. The extensometer used to measure elongation had a gauge length of 50 mm (A50).

Table 1. Mechanical properties of steel sheet.

Steel Sheet	Thickness (mm)	Yield Strength R_e (MPa)	Tensile Strength R_m (MPa)	Hardness (HV0.1)	Elongation (%)	Reduction in Area [%]	n-Value (-)
JSC1180	1.20	939	1209	421	8.0	40.5	0.135

The shearing conditions of the specimens are shown in Figure 4, and the resistance spot welding conditions and weld details in Figure 5. The blanks were then sheared with a die mounted on a servo press (Amada press systems Co., Ltd., SDE-8018, Isehara, Japan). TiN-coated SKH51 punches and dies were used. The material of the blank holder was SS400 without a coating. The sheets were fixed to the die via a blank holder bolted to the die, and a urethane rubber counter block was attached to the lower part of the punch to suppress burrs. The punch speed was 90 mm/s, the shear angle of the punch was 0°, and the clearance ratio to sheet thickness was 10%. The conditions for resistance spot welding were set to satisfy JIS standards [31]. B-grade conditions (nugget diameter: 4.4 mm; tensile shear load: 10.3 kN). The actual average nugget diameter was 5.7 mm, and the average tensile shear strength was 20.26 kN. There was no difference in hardness distribution in the width and thickness directions for welds welded under different cutting edge conditions.

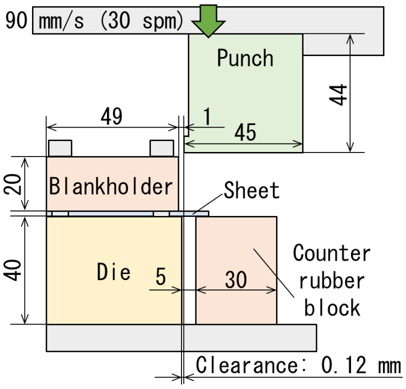

Figure 4. Shearing conditions of sheet.

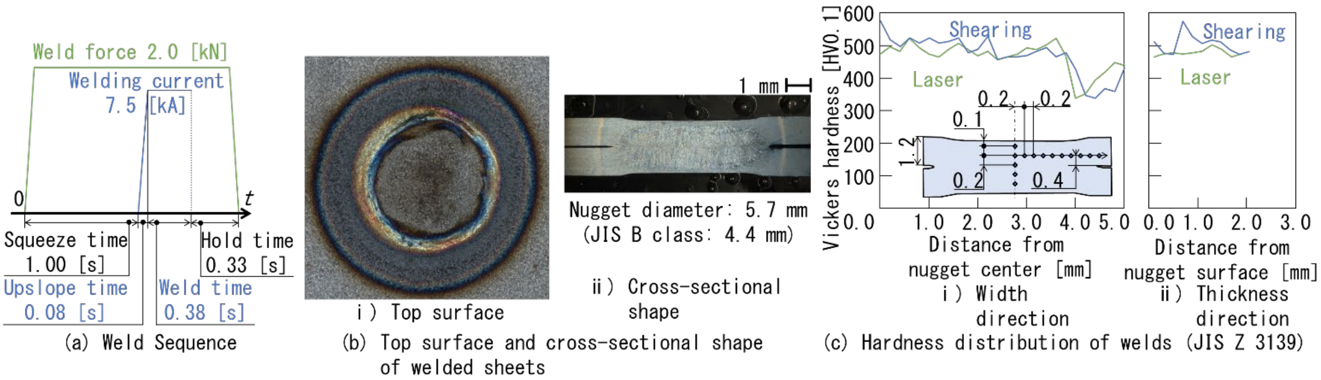

Figure 5. (**a**) Conditions for resistance spot welding; (**b**) surface and sectional details of the weld; and (**c**) hardness distribution in welds.

The dimensions of the specimens used for testing are shown in Figure 6. Specimens conforming to JIS standards [32] were used to measure the steel sheet strength. The specimens were hydrogen embrittled via cathodic hydrogen charging, and the steel sheet strength after hydrogen embrittlement was obtained. In the tensile shear test, specimens based on JIS standards [33] were used. Two 30 mm × 100 mm steel sheets were welded together in a stack. In shear fatigue tests, specimens based on JIS standards [34] were used. Two 40 mm × 140 mm steel sheets were welded together in a stack. The sheets, having an overlap length L, were welded under three conditions of L = 40, 15, and 10 mm. The sheets were resistance spot-welded to the center of the overlap length. The cut edge near the weld had sheared and laser-cut surfaces. All other edges except for near the weld were laser-cut.

To penetrate hydrogen into the specimen, accelerated tests were conducted using the cathodic hydrogen charge method. The cathodic hydrogen charge test method is shown in Figure 7. The specimens were immersed in a 3.0 g/L NH_4SCN solution containing 3 vol% NaCl, and the temperature of the solution was maintained at 30–35 °C. An Ag/AgCl electrode was used as the reference electrode, the test specimen as the working electrode, and a Pt electrode as the counter electrode. The test time was defined as the charge time T. Various tests were performed on specimens that had been hydrogen-charged for 24 h and on specimens that had not been hydrogen-charged.

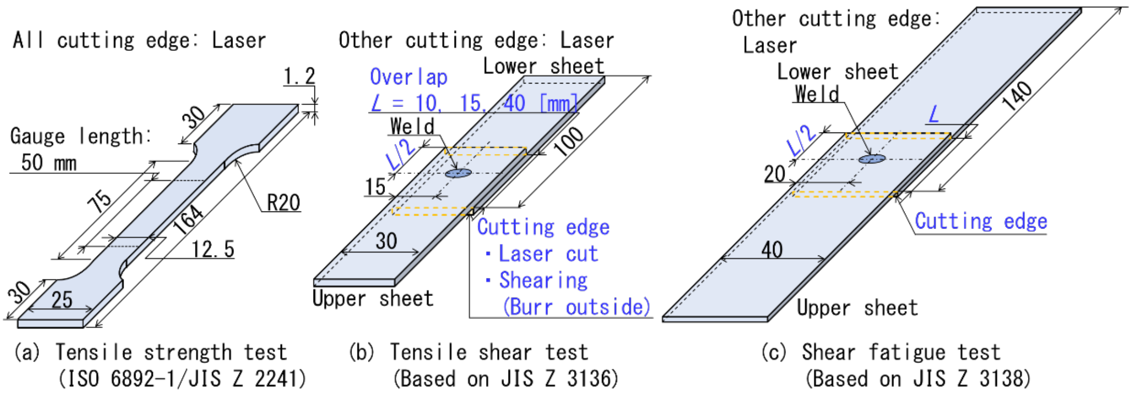

Figure 6. (**a**) Specimen for tensile strength test of steel sheet; (**b**) specimen for tensile shear test of welds; and (**c**) specimen for shear fatigue test of welds.

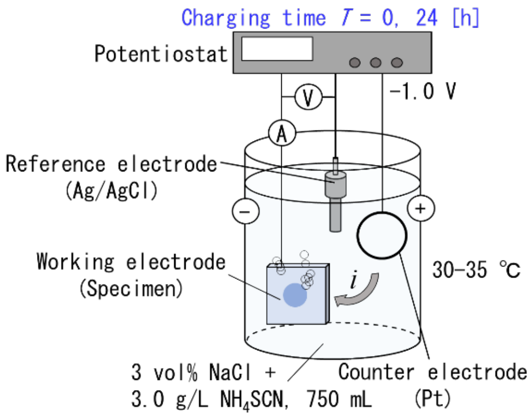

Figure 7. Cathodic hydrogen charge test method.

The test method for shear fatigue testing is shown in Figure 8. The specimens were mounted on a servohydraulic fatigue testing machine (Shimadzu Corporation, EHF-UV050k, Kyoto, Japan) in a room with a room temperature of 23 ± 2 °C and a humidity of 60 ± 5%, and a sinusoidal repeated load was applied at 40 Hz. A repeated load F and A repeated maximum load F_{max} were defined, where F_{max} was varied between 1 kN and 5 kN, approximately 5% to 25% of the tensile shear strength in the static test, and the endurance limit N_{max} was set to 10^6 cycles.

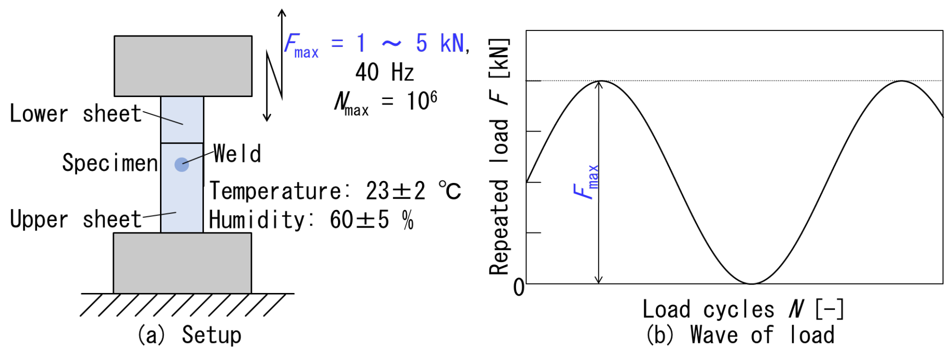

Figure 8. (**a**) Test conditions for shear fatigue testing and (**b**) waveform of load and definition of repeated load F in shear fatigue testing.

3. Results

3.1. Sheared Edge and Tensile Strength of Steel Sheets

Laser and shear cutting surfaces and the quality of the sheared edge of the cut sheet are shown in Figure 9. The entire surface of the laser-cut edge was the heat-affected zone

(HAZ), and no dross was generated. The sheared edge consisted of a rollover, a burnished surface, a fracture surface, and a burr. To avoid weld defects due to burr bumps, they were welded on top of each other with the rollover side in contact during welding.

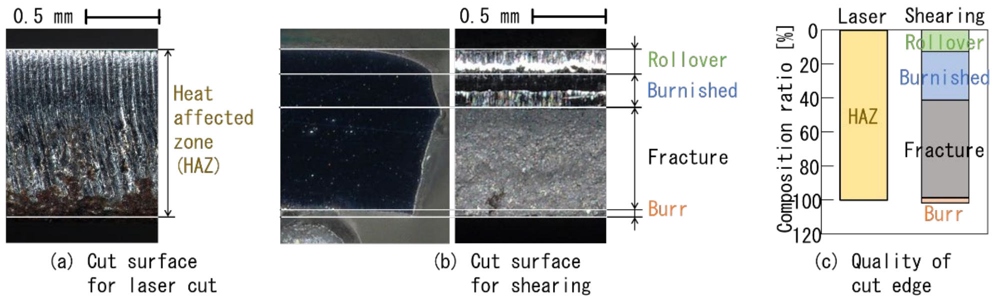

Figure 9. (**a**) Laser-cut edge and (**b**) shear edge, and (**c**) composition ratio for each cut surface.

The cut edges at charging time T = 24 h are shown in Figure 10. The cut edge of the welded specimen was observed before the tensile test. Regardless of overlap length, cracks occurred in fracture surfaces at the sheared edges, although no cracks were observed at the laser-cut edges.

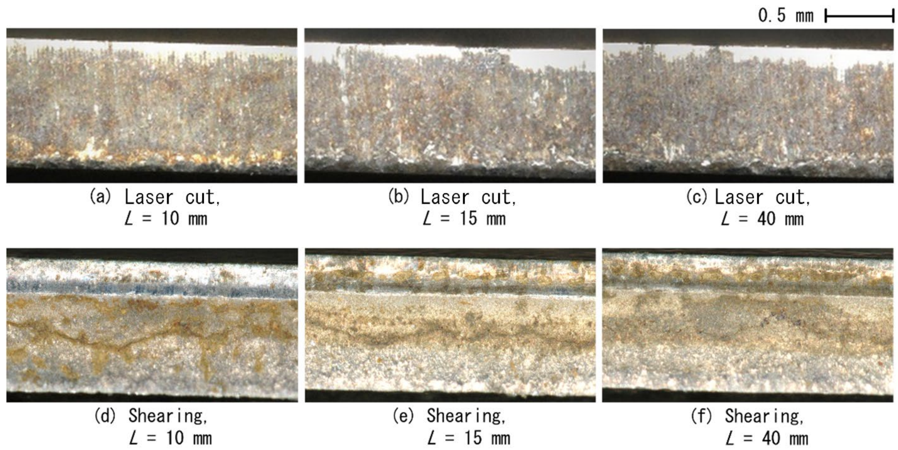

Figure 10. Cut edges at T = 24 h for (**a**–**c**) laser-cut and (**d**–**f**) sheared edges.

The load–stroke curves of the hydrogen-charged steel sheet in a tensile test and the specimen after fracture are shown in Figure 11. The elongation at the break in the hydrogen-charged steel sheet was approximately 10% lower than that of the non-hydrogen-charged steel sheet, but the fracture shape did not change.

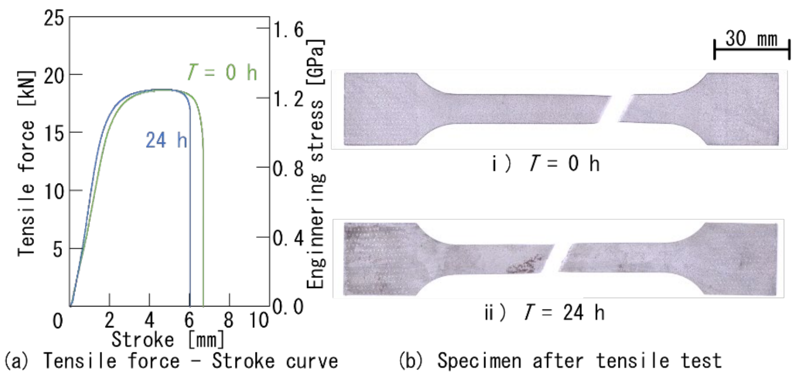

Figure 11. (**a**) Tensile force—stroke diagram at charge times T = 0 and 24 h, and (**b**) specimen after fracture at charge times T = 0 and 24 h.

3.2. Tensile Shear Test Results of Hydrogen-Charged Resistance Spot Welds

The tensile shear force–stroke curves for tensile shear tests of hydrogen-charged resistance spot welds for each cut edge are shown in Figure 12. Although a deviation in the curves was observed, typical curves are shown in this figure. The load increases with increasing the stroke. The peak of the increased load is shown, and then they drop suddenly. In the both cut edges, the peak load and the stroke at the peak tend to be decreased with decreasing the overlap length with hydrogen charge. The reductions in the peak load and the stroke might be caused by the reduced ductility of the hydrogen charged material.

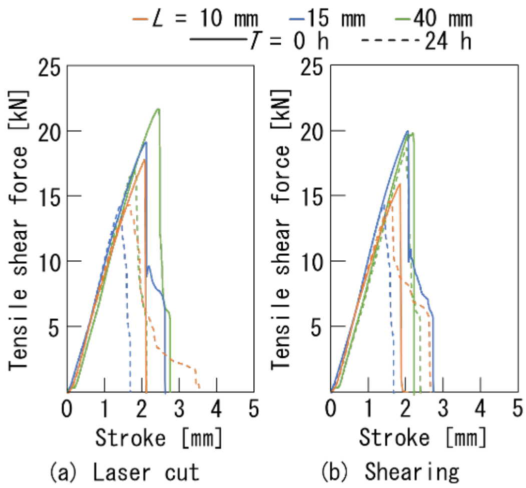

Figure 12. Tensile shear force—stroke curves for (**a**) laser-cut edge and (**b**) sheared edge.

The failure modes of the tensile shear specimens are shown in Figure 13. The failure mode for L = 40 mm and 15 mm was plug failure for both cut edges with and without hydrogen charge. The failure mode for L = 10 mm was shear failure toward the cutting edge for both cut edges with and without hydrogen charge. This is due to the crack growing from the nugget edge toward the cut edge because of the small overlap length. There were no effects of cut edges or hydrogen charge on the fracture mode. However, cracks due to hydrogen embrittlement were observed at the interface between the nugget and heat-affected zone on the surface of the weld.

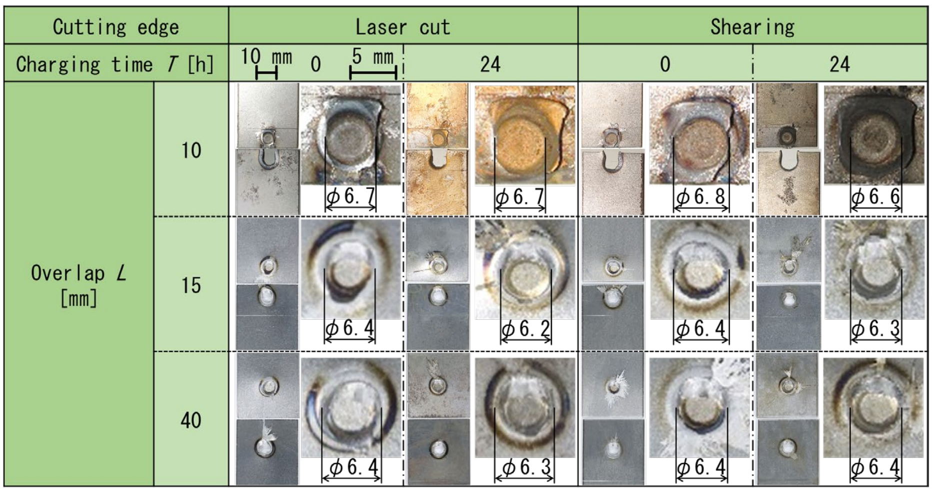

Figure 13. Failure mode of the tensile shear specimen.

The tensile shear strength in the tensile shear tests of the hydrogen-charged resistance spot welds for each cutting edge and the strength ratio at T = 24 and 0 h are shown in Figure 14. In the both laser-cut and sheared edge conditions, the ratio in tensile shear strength decreased with decreasing the overlap length. The minimum ratio in tensile shear strength in the laser-cut specimen was approximately 80%, whereas the minimum ratio in the sheared specimen was approximately 75%. This reduction may be due to cracking at the sheared edge in addition to hydrogen embrittlement of the material.

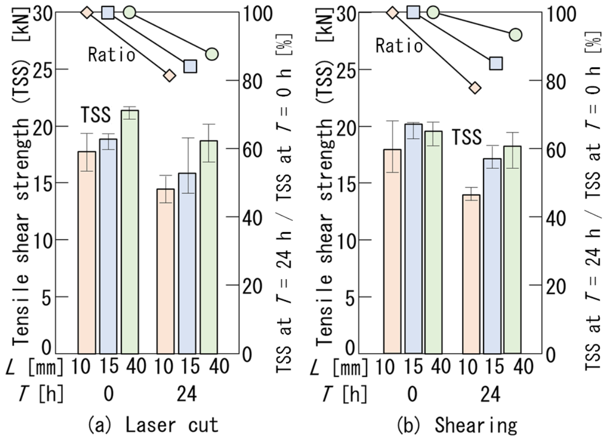

Figure 14. Tensile shear strength in tensile shear tests of hydrogen-charged resistance spot welds and strength ratio at T = 24 and 0 h for (**a**) laser cut and (**b**) shearing.

3.3. Shear Fatigue Test Results of Hydrogen-Charged Resistance Spot Welds

The classification of failure modes in the specimen after shear fatigue testing is shown in Figure 15. The following four failure modes were observed and classified in the specimens after fatigue testing:

1. Without fracture: no fracture occurs even after the test is run up to the endurance limit.
2. Fracture in width direction: cracks occur at the nugget edge and extend in the direction of the sheet width, and then fracture.
3. Fracture in cutting edge: cracks occur at the nugget edge and extend from the direction of the sheet width to the direction of cutting edge, and then fracture.
4. Plug failure: cracks occur at the nugget edge and extend along the heat-affected zone, and then fracture.

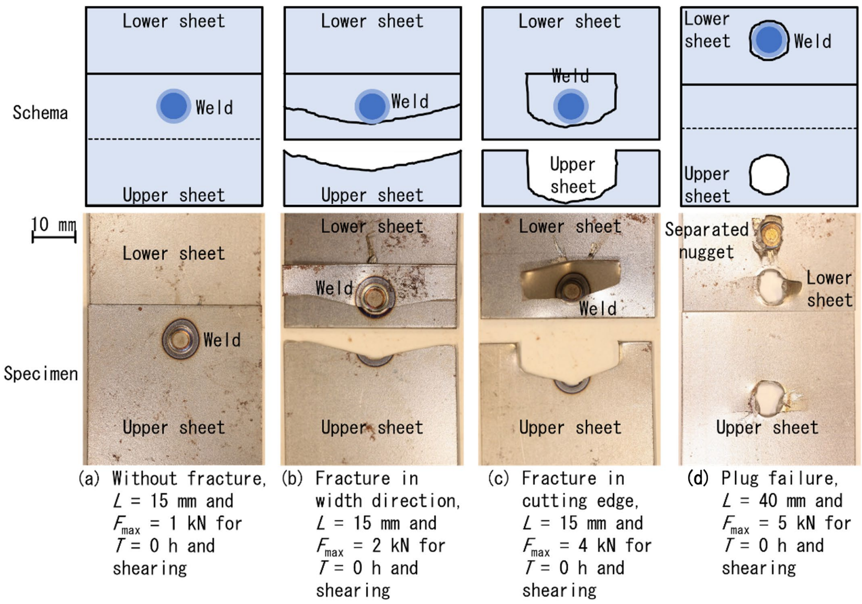

Figure 15. (**a**) No fracture after 10^6 tests, (**b**) crack grows in direction of sheet width, (**c**) crack grows in the direction of cutting edge from sheet width direction, and (**d**) crack grows along heat-affected zone.

The fatigue limit and the failure mode for each cut edge for repeated loads F_{max} are shown in Figure 16. The fatigue test was performed three times. The plots indicate the mean values, and the error bars indicate the minimum and maximum values. Regardless of the cut edge, the fatigue limit at failure occurred tends to decrease with decreasing overlap length. The failure modes without fracture and with fracture in the width direction in small repeated load changed to fractures in the cut edge and plug failure in large repeated load. The fatigue limit of the hydrogen-charged specimens was lower than that of the non-hydrogen-charged specimens.

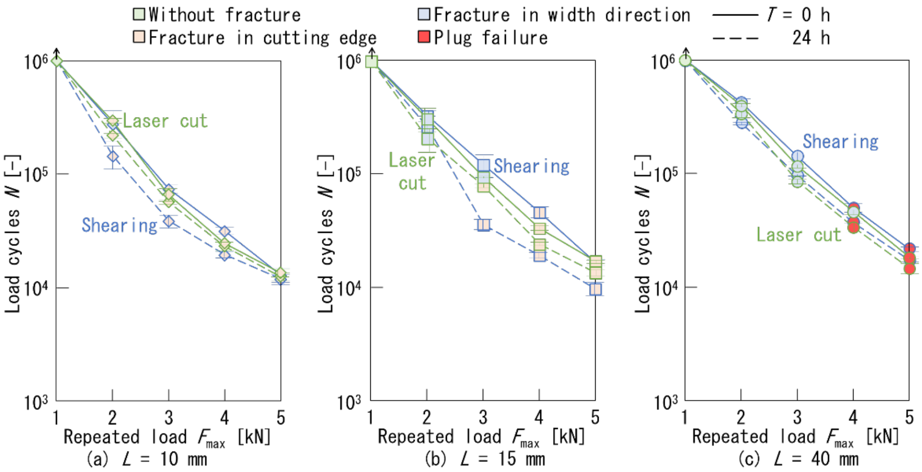

Figure 16. Fatigue limit and the failure mode for repeated load F_{max}: fatigue limits and failure modes of tensile fatigue specimens with (**a**) L = 10 mm, (**b**) L = 15 mm, and (**c**) L = 40 mm.

The ratio of the fatigue limits before and after hydrogen charging for each cut edge is shown in Figure 17. The ratio in the fatigue limit was calculated from the mean reduction from the fatigue test in Figure 16. The ratios in some conditions are smaller than those in the static test in Figure 14. The fatigue limit was decreased after hydrogen charging except for F = 1 kN, and then the ratio in fatigue limit for the sheared edges tended to be larger than for the laser-cut surface edges. The minimum ratio for the sheared edges is about 30%, whereas the ratio for the laser-cut edges is about 65%. For the sheared edge, where L = 15 mm and F_{max} = 3 kN, the minimum ratio in fatigue limit was observed, and then the failure mode was changed from fracture in the width direction to fracture in the cut edge. As shown in these results, the fatigue limit for the sheared edge was affected by the overlap length and hydrogen charging with changing failure mode.

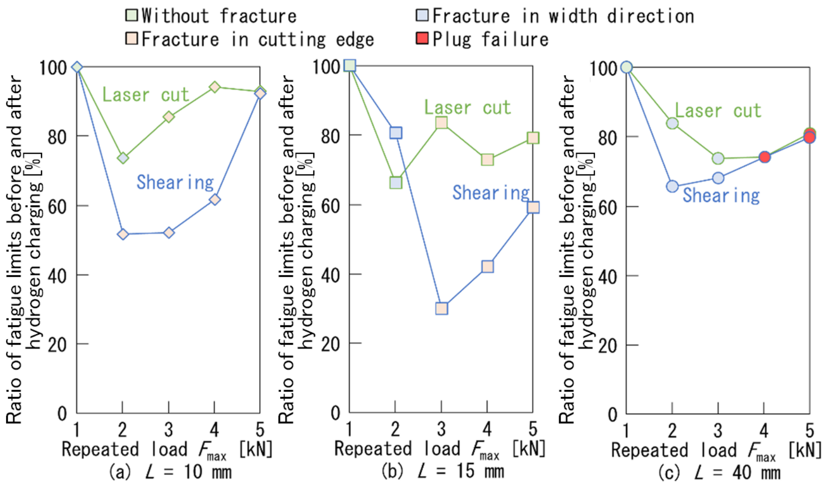

Figure 17. Ratio of fatigue limits and failure mode for repeated load F_{max} at (**a**) L = 10 mm, (**b**) L = 15 mm, and (**c**) L = 40 mm.

The fracture modes before and after hydrogen charging for each cut edge at L = 15 mm and F_{max} = 3 kN are shown in Figure 18. In the laser-cut edge, the fracture mode was fracture in the width direction regardless of whether hydrogen charging was applied or not. On the other hand, in the sheared edge, the fracture mode was in the width direction at T = 0 h, while it changed to fracture in the cut edge at T = 24 h. The fatigue limit in the laser-cut edge shortened with the same fracture mode with the hydrogen charge, whereas the fatigue limit in the sheared edge was greatly reduced by the change in failure mode due to the effect of cracks at the sheared edge, as shown in Figure 10.

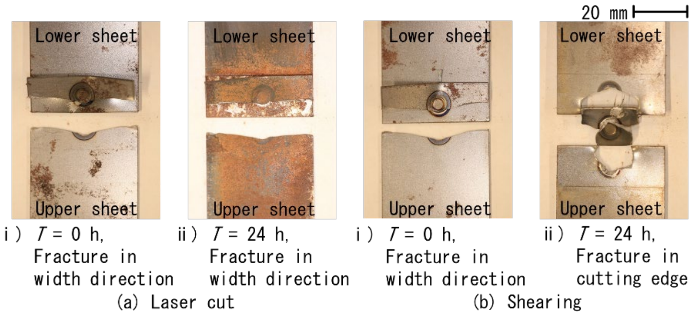

Figure 18. Fracture modes for each cutting edge at L = 15 mm and F_{max} = 3 kN.

4. FEM Stress Concentration Analysis and Discussion of Results

The specimens with shear surfaces showed a greater reduction in fatigue limit after hydrogen charging. Among them, the ratio in fatigue limit was the highest at L = 40 mm and the lowest at L = 15 mm. At F_{max} = 3 kN, the reduction in fatigue limit due to the difference in the cut edge was small at L = 40 mm, and it was the largest at L = 15 and 10 mm. To discuss this point, the stress distributions occurring in the sheets were obtained from the analysis.

The analysis and material conditions in the static–elastic finite element analysis are shown in Table 2, and the analysis model is shown in Figure 19. For investigation of the stress distribution in the sheet at F = 3 kN in the shear test, the static analysis in SolidWorks 2019 was used. In this model, the nugget was a rigid cylinder with a diameter of 5.4 mm and the sheets were assumed as elastic solid elements. The effects of cut edges, hydrogen charge, and fracture criteria were not considered in the model. Because cracks generally occur around the nugget, the distributions of stress on the interface between the sheets were evaluated.

Table 2. Analysis and material conditions.

Software	**Analysis Mode**	**Applied Force *F* (kN)**	**Element Type**	**Mesh Size (mm)**
SolidWorks 2019	Static	3.0	Solid	2.25
Elastic modulus (MPa)	**Poisson's ratio (-)**	**Mass density (kg/m^3)**	**Tensile strength (MPa)**	**Yield stress (MPa)**
210,000	0	7900	1209	800

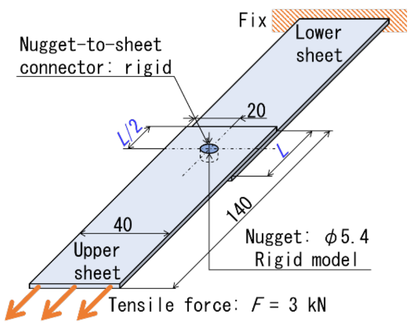

Figure 19. Analysis model for stress analysis.

The distribution of the maximum principal stress on the upper surface in the lower sheet is shown in Figure 20. High maximum principal tensile stress occurred around the nugget. This result is consistent with the fact that fracture occurs close to the nugget. The maximum principal stress distributions at L = 10 and 15 mm, where the overlap is short, are almost the same. However, at L = 10 mm, the maximum principal tensile stress is distributing to the cutting edge. This difference in distribution is likely to cause the difference in the fracture rates at the cut edges in fatigue tests.

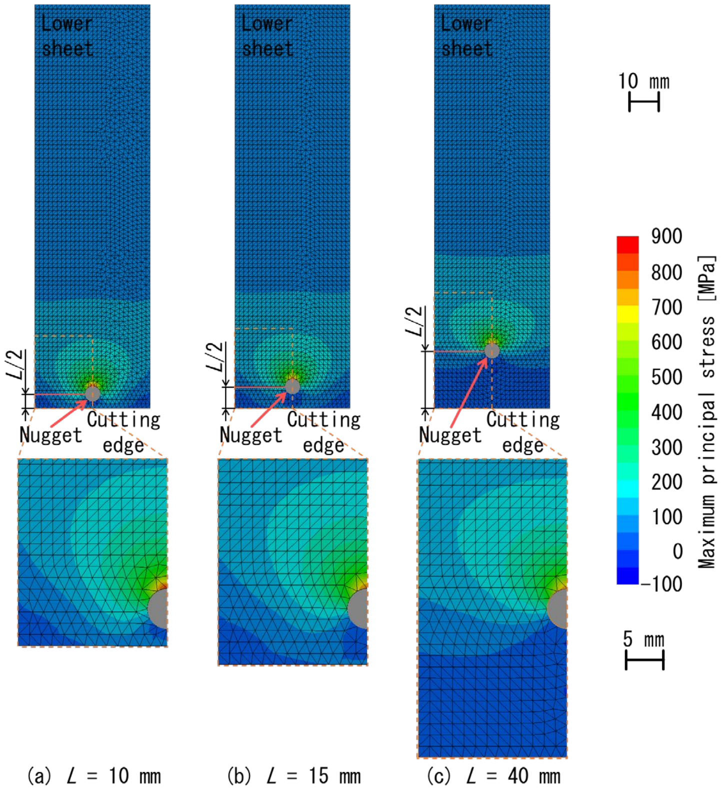

Figure 20. Maximum principal stress distribution at F = 3 kN on upper surface in lower sheet at (**a**) L = 10 mm, (**b**) 15 mm, and (**c**) 40 mm.

The relationship between the overlap length and the failure mode is shown in Figure 21. When the overlap length is large, the stress in the width direction increases in Figure 20c. Cracks grow in the width direction due to the longer distance from the cut edge. The effect of the cut edge is also smaller. After hydrogen embrittlement, the effect of the sheared edge is also small because of its long distance from the crack. On the other hand, when the overlap length is small, the stress in the direction of the sheared edge increases. The cracks change direction in the cutting edge direction because the distance to the sheared edge is short and the shear deformation stress in the cutting edge direction is smaller than the stress that grows the crack in the width direction. Hydrogen embrittlement has a greater effect because it tends to merge with cracks at the sheared edge. At L = 15 mm, the middle length, the difference in stress between the width direction and the cutting edge direction becomes smaller, and the crack growth direction changes more easily. In addition, the crack growth direction is more likely to change because it is closer to the sheared edge and more sensitive to the effects of hydrogen embrittlement. Therefore, when the crack growth direction changes, the fatigue limit decreases significantly due to hydrogen embrittlement because the reduction in the fatigue limit becomes large.

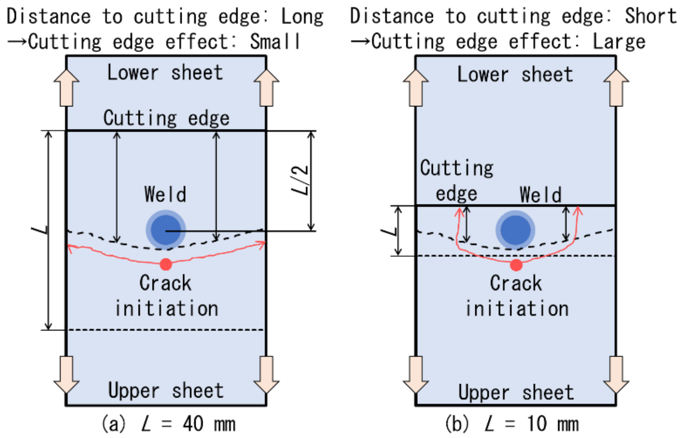

Figure 21. Relationship between overlap length and failure mode at (**a**) large overlap length and (**b**) small overlap length.

5. Conclusions

In this paper, the effects of the sheared edge and the overlap length on the reduction in the tensile fatigue limit after hydrogen embrittlement of resistance spot-welded ultra-high-strength steel sheets were investigated, with the following results:

1. In tensile shear deformation of resistance spot welds of ultra-high-strength steel sheets, the maximum load decreased as the overlap length decreased. Furthermore, the reduction in maximum load increased with the decreasing overlap length when the weld was hydrogen-charged.
2. In the fatigue test of resistance spot welds of ultra-high-strength steel sheets, the fatigue limit decreased with decreasing the overlap length under the same load. In the sheared edge, the fatigue limit was reduced due to the reduction in material ductility and cracking at the sheared edges caused by hydrogen embrittlement.
3. For the fatigue limit of resistance spot welds with a sheared edge, the reduction in the fatigue limit due to hydrogen charging was larger than that of a laser-cut edge. In particular, the fatigue limit of the resistance spot weld with a sheared edge decreased significantly when the fracture mode was changed.
4. The change in the fatigue limit due to hydrogen charging was larger in welds with a small overlap length where the fracture mode was likely to change.
5. If the distance between the sheared edge and the weld was not sufficient, the fatigue limit, whose failure mode changed due to hydrogen charging, was more sensitive to the sheared edge than to static loads, which might cause a significant reduction in the fatigue limit, and should be considered in the design of welded joints.
6. If the sheared edge is close to the weld, there may be a significant reduction in fatigue strength due to long-term use, so an appropriate overlap length must be selected.

Author Contributions: Conceptualization, R.Y. and Y.A.; methodology, investigation, visualization, writing—original draft preparation, R.Y.; supervision, Y.A. All authors have read and agreed to the published version of the manuscript.

Funding: This research received no external funding.

Institutional Review Board Statement: Not applicable.

Informed Consent Statement: Not applicable.

Data Availability Statement: All data are available from the corresponding author upon reasonable request. The data are not publicly available due to privacy reason.

Acknowledgments: The authors would like to thank Naoto Sakuraba and Hiroki Kikukawa for their great support and fruitful discussions in the experiment.

Conflicts of Interest: The authors declare no conflict of interest.

References

1. Billur, M.S.; Altan, T. Challenges in forming advanced high strength steels. In Proceedings of the New Developments in Sheet Metal Forming, Sttutgart, Germany, 2–4 May 2012; pp. 285–304.
2. Mori, K.; Akita, K.; Abe, Y. Springback behaviour in bending of ultra-high-strength steel sheets using CNC servo press. *Int. J. Mach. Tools Manuf.* **2007**, *47*, 321–325. [CrossRef]
3. Kaupper, M.; Merklein, M. Bendability of advanced high strength steels—A new evaluation procedure. *CIRP Ann. Manuf. Technol.* **2013**, *62*, 247–250. [CrossRef]
4. Abe, Y.; Ohmi, T.; Mori, K.; Masuda, T. Improvement of formability in deep drawing of ultra-high strength steel sheets by coating of die. *J. Mater. Process. Technol.* **2014**, *214*, 1838–1843. [CrossRef]
5. Mori, K.; Abe, Y.; Sedoguchi, K. Delayed fracture in cold blanking of ultra-high strength steel sheets. *CIRP Ann. Manuf. Technol.* **2019**, *68*, 297–300. [CrossRef]
6. Li, X.; Ma, X.; Zhang, J.; Akiyama, E.; Wang, Y.; Song, X. Review of Hydrogen Embrittlement in Metals: Hydrogen Diffusion, Hydrogen Characterization, Hydrogen Embrittlement Mechanism and Prevention. *Acta Metall. Sin-Engl.* **2020**, *33*, 759–773. [CrossRef]
7. Venezuela, J.; Zhou, Q.; Liu, Q.; Li, H.; Zhang, M.; Dargusch, M.S.; Atrens, A. The influence of microstructure on the hydrogen embrittlement susceptibility of martensitic advanced high strength steels. *Mater. Today Commun.* **2018**, *17*, 1–14. [CrossRef]
8. Liu, M.A.; Rivera-Diaz-del-Castillo, P.E.J.; Barraza-Fierro, J.I.; Castaneda, H.; Srivastava, A. Microstructural influence on hydrogen permeation and trapping in steels. *Mater. Des.* **2019**, *167*, 107605. [CrossRef]
9. Liu, Y.i.; Chen, Y.; Yang, C.; Han, X. Study on hydrogen embrittlement and reversibility of hot-stamped aluminized 22MnB5 steel. *Mater. Sci. Eng. A* **2022**, *848*, 143411. [CrossRef]
10. Matsuda, H.; Kitani, Y.; Matsushita, M.; Taniguchi, K.; Sawanishi, C.; Ikeda, R. Development of Welding Technologies for Automotive Body. *Jfe Tech. Rep.* **2019**, *24*, 52–60.
11. Furusako, S.; Matsui, S.; Zeniya, T.; Wakabayashi, C.; Okada, T.; Shimada, N.; Fujimoto, H. Assembly Technology of Welding and Joining for Ultra-high Strength Steel Sheets for Automobiles—Spot Welding—. *Nippon. Steel Tech. Rep.* **2019**, *122*, 65–75.
12. Muhmud, K.; Murugan, S.P.; Cho, Y.; Ji, C.; Nam, D.; Park, Y. Geometrical degradation of electrode and liquid metal embrittlement cracking in resistance spot welding. *J. Manuf. Process.* **2021**, *61*, 334–348. [CrossRef]
13. Di Giovanni, C.; He, L.; Pistek, U.; Goodwin, F.; Biro, E.; Zhou, N.Y. Role of spot weld electrode geometry on liquid metal embrittlement crack development. *J. Manuf. Process.* **2020**, *49*, 1–9. [CrossRef]
14. Ling, Z.; Wang, M.; Kong, L.; Chen, K. Towards an explanation of liquid metal embrittlement cracking in resistance spot welding of dissimilar steels. *Mater. Des.* **2020**, *195*, 109055. [CrossRef]
15. Kalashami, A.G.; Di Giovanni, C.; Razmpoosh, M.H.; Goodwin, F.; Zhou, N.Y. The effect of silicon content on liquid-metal-embrittlement susceptibility in resistance spot welding of galvanized dual-phase steel. *J. Manuf. Process.* **2020**, *57*, 370–379. [CrossRef]
16. Kalashami, A.G.; Han, X.; Goodwin, F.; Zhou, N.Y. The influence of modified annealing during the galvanizing process on the resistance spot welding of the CMn1.8Si advanced high strength steel. *Surf. Coat. Technol.* **2020**, *381*, 125181. [CrossRef]
17. Lee, H.; Jo, M.C.; Sohn, S.S.; Kim, S.; Song, T.; Kim, S.; Kim, H.S.; Kim, N.J.; Lee, S. Microstructural evolution of liquid metal embrittlement in resistance-spot-welded galvanized TWinning-Induced Plasticity (TWIP) steel sheets. *Mater. Charact.* **2019**, *147*, 233–241. [CrossRef]
18. Colombo, T.C.A.; Rego, R.R.; Otubo, J.; de Faria, A.R. Mechanical reliability of TWIP steel spot weldings. *J. Mater. Process. Technol.* **2019**, *266*, 662–674. [CrossRef]
19. Liu, X.; Wei, Y.; Wu, H.; Zhang, T. Factor analysis of deformation in resistance spot welding of complex steel sheets based on reverse engineering technology and direct finite element analysis. *J. Manuf. Process.* **2020**, *57*, 72–90. [CrossRef]
20. Pasarkar, A.; Mane, A.; Singh, N.; Datarkar, A.; Raut, N. A Review of fatigue behaviour of resistance spot welds. *Res. Eng. Struct. Mater.* **2023**, *9*, 181–194. [CrossRef]
21. Ordonez, J.H.; Ambriz, R.R.; Garcia, C.; Plascencia, G.; Jaramillo, D. Overloading effect on the fatigue strength in resistance spot welding joints of a DP980 steel. *Int. J. Fatigue.* **2019**, *121*, 163–171. [CrossRef]
22. Cho, H.; Nam, S.; Hwang, I.; Oh, J.H.; Kang, M.; Kim, Y. Fatigue Behaviors of Resistance Spot Welds for 980 MPa Grade TRIP Steel. *Metals* **2019**, *9*, 1086. [CrossRef]
23. Linder, J.; Melander, A.; Larsson, M.; Bergengren, Y. Fatigue Design of Spot-Welded Austenitic and Duplex Stainless Sheet Steels. *Fatigue. Fract. Eng. Mater. Struct.* **1998**, *21*, 673–686. [CrossRef]
24. Linder, J.; Melander, A. Fatigue strength of spot welded stainless sheet steels exposed to 3% NaCl solution. *Int. J. Fatigue.* **1998**, *20*, 383–388. [CrossRef]
25. Vural, M.; Akkuş, A.; Eryürek, B. Effect of welding nugget diameter on the fatigue strength of the resistance spot welded joints of different steel sheets. *J. Mater. Process. Technol.* **2006**, *176*, 127–132. [CrossRef]
26. Long, X.; Khanna, S.K. Fatigue properties and failure characterization of spot welded high strength steel sheet. *Int. J. Fatigue.* **2007**, *29*, 879–886. [CrossRef]
27. Ren, S.; Ma, N.; Tsutsumi, S.; Watanabe, G.; He, H.; Cao, C.; Huang, L. Post-weld cold working for fatigue strength improvement of resistance spot welded joint of advanced high-strength steel. *J. Mater. Process. Technol.* **2022**, *299*, 117364. [CrossRef]

28. Tanegashima, R.; Akebono, H.; Sugeta, A. Fatigue life estimation based on fracture mechanics of single spot welded joints under different loading modes. *Eng. Fract. Mech.* **2017**, *175*, 115–126. [CrossRef]
29. Li, X.; Gong, B.; Deng, C.; Li, Y. Failure mechanism transition of hydrogen embrittlement in AISI 304 K-TIG weld metal under tensile loading. *Corros. Sci.* **2018**, *130*, 241–251. [CrossRef]
30. Sun, Y.; Fujii, H.; Imai, H.; Kondoh, K. Suppression of hydrogen-induced damage in friction stir welded low carbon steel joints. *Corros. Sci.* **2015**, *94*, 88–98. [CrossRef]
31. *JIS Z 3140*; Method of Inspection and Acceptance Levels for Resistance Spot Welds. Japanese Standards Association: Tokyo, Japan, 2017.
32. *JIS Z 2241*; Metallic Materials—Tensile Testing—Method of at Room Temperature. Japanese Standards Association: Tokyo, Japan, 2022.
33. *JIS Z 3136*; Specimen Dimensions and Procedure for Shear Testing Resistance Spot and Embossed Projection Welded Joints. Japanese Standards Association: Tokyo, Japan, 1999.
34. *JIS Z 3138*; Method of Fatigue Testing for Spot Welded Joint. Japanese Standards Association: Tokyo, Japan, 1989.